RSC Advances

ROYAL SOCIETY OF CHEMISTRY

www.rsc.org/advances

Journal Name

RSCPublishing

ARTICLE

Computational modelling of the enantioselectivity in the asymmetric 1,4-addition reaction catalyzed by a Rh complex of a *S*-chiral disulfoxide

Cite this: DOI: 10.1039/x0xx00000x

Received 00th January 2012,
Accepted 00th January 2012

DOI: 10.1039/x0xx00000x

www.rsc.org/

You-Gui Li,*[a] Li Li,[a] Ming-Yue Yang,[a] Hua-Li Qin[b] and Eric Assen B. Kantchev*[a,c]

Computational chemistry is a powerful tool for understanding of chiral catalysis and aiding future catalyst design. Here we present a DFT (PCM/PBE0/DGDZVP) modelling of the enantioselective step in the 1,4-addition of phenylboronic acid to 5 Michael acceptors catalyzed Rh ligated with a disulfoxide ligand whose only source of chirality is the sulfur atoms. For all substrates, the predicted absolute configuration was in agreement with the experiment. Using the dispersion-interaction-corrected SMD/M06 method improved the quantitative agreement of predicted and experimental %ee values (within 0.2-0.7 kcal mol^{-1}). The steric high pressure exerted by the bulky *tert*-butyl groups is the primary determinant of the enantioselectivity.

Introduction

Discovery of chiral ligands for transition metal-catalyzed asymmetric reactions is one of the most important endeavours in current organic chemistry research.[1] These ligands not only serve to transfer chirality to the reactants in the enantiodiscriminating step, but also modulate the steric and electronic behaviour of the metal to ensure high catalyst activity and productivity. The synthetically important[2, 3] Rh-catalyzed 1,4-addition of arylboronic acids to α,β-unsaturated ketones[4] such as 2-cyclohexenone (**1**; Figure 1a) provides an excellent illustration of this principle: the initial (in 1998) high yields and enantioselectivities with binap as the ligand (**I**; binap = 2,2-diphenylphosphino-1,1-binaphthyl)[5] were improved while simultaneously increasing the reaction rate by a conceptually new ligand[6] specially developed for this transformation (in 2003), Phbod (**II**, Phbod = 2,5-diphenylbicycloocta[2.2.2]-2,5-diene). Due to their higher activity,[7] diene ligands have by and large replaced diphosphanes as the ligands of choice in the 1,4-addition and related arylation reactions.[3, 8] In 2008, Dorta et al. introduced atropisomeric biaryl-based chiral sulfoxides[9, 10] (analogues of binap; e.g., **III**) in the 1,4-addition reaction, which showed levels of performance that was considerably higher than diphosphanes and at par or even exceeding that of chiral dienes.

Explanation of the mechanism of action of chiral ligands goes hand in hand with discovery efforts. Based on the X-ray structure of [(binap)PdCl$_2$] acquired in their investigation of a mechanistically related enantioselective Heck-Mizoroki reaction,[11] Hayashi et al. proposed a pictorial model explaining the observed enantioselectivity by the avoidance of the steric clash of the ketone substituent and the large group (e.g., Ph in **I**[5] and **II**[12]) on the ligand (Figure 1b). Due to the excellent predictive power, visual appeal and intellectual elegance of this model, adaptations to different ligands and substrates have appeared in numerous of papers on Rh-catalyzed 1,4- additions

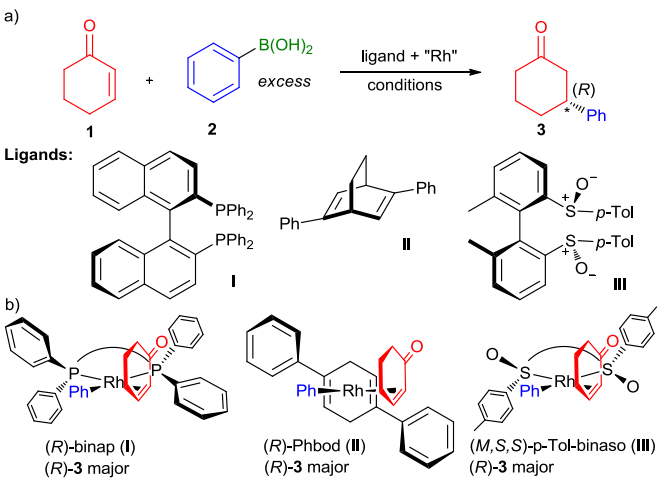

Figure 1. (a) The asymmetric Rh-catalyzed 1,4-addition reaction and representative diphosphane,[5] diene,[12] and disulfoxide ligands[10] showing high yields and enantioselectivities therein. (b) Pictorial models rationalizing the formation of the major enantiomer by avoiding steric repulsion with the forward-facing Ph group (diphosphane and diene) or dipole-dipole repulsion with the negatively charged oxygen atom (disulfoxide).

in recent years.[10, 13, 14] Computational modelling provides a powerful alternative to pictorial models because, being based on first principles, is not only theoretically sound but also permits quantitative evaluation of the enantioselectivity, which is much more important than simply predicting the reaction course. Recent DFT investigations of the origin of the enantioselectivity of bidentate phosphane,[15, 16] diene[15, 17, 18] and disulfoxide[19] ligands have shown that the Hayashi models quite

accurately represent the structures of the enantiodiscriminating carborhodation transition state (CR-TS).

Until Dorta's work, chiral sulfoxide ligands had been used sporadically in various catalytic asymmetric reactions, usually showing uncompetitive levels of performance compared to other ligand classes.[20] Dorta's discovery reignited the field and subsequent studies from various groups[14, 21, 22] have solidified the position of chiral disulfoxide as excellent ligands for the Rh-catalyzed 1,4-addition. Particularly, a ligand developed by Liao et al.[22] (**IV**; Scheme 1) is distinguished by uniformly high levels of enantioselectivity for a wide range of substrates achieved solely by the sulfoxide chirality. A computational study of the origin of the selectivity for ligand **IV** by density functional theory (DFT) is presented herein.

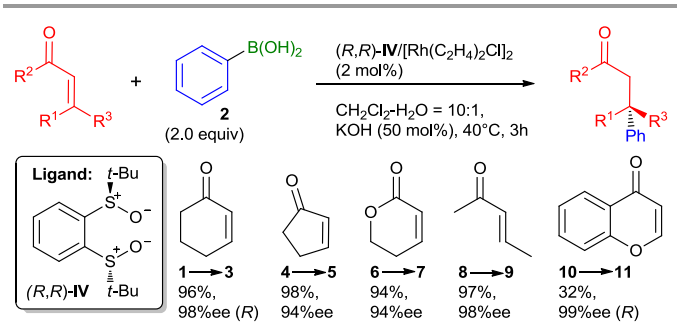

Scheme 1. The previously published 1,4-aryltaion reaction mediated by (*R,R*)-**IV**/Rh.[22] The absolute configuration of products **3** and **11** were assigned based on literature data. For **11**, 5 mol% Rh and 3.0 equiv. **2** over 5h were required.

Results and discussion

The accepted catalytic cycle[23] of the 1,4-arylation (Scheme 1) comprises of transmetalation (TM), enone binding (EB), carborhodation (CR) and Rh-enolate hydrolysis (EH) steps, with the CR step being the one where the enantiodiscrimination takes place (Scheme 2). The reaction profile (Figure 2a) for the EB+CR steps was calculated[24] with the Perdew-Burke-Ernzerhof hybrid generalized gradient approximation (hGGA) functional containing 25% Hartree-Fock exchange (PBE0)[25] combined with the full-electron, DFT-optimized DeGauss double-ζ+valence polarization basis set (DGDZVP)[26] designed to give low basis set superposition error (BSSE). All structures were optimized in implicit CH_2Cl_2 by the integral equation formalism variant of the polarisable continuum model (IEFPCM)[27] and the frequency calculations were performed at 40°C (313.15K) to obtain the vibrational partition function hence ΔS and ΔG values at the reaction temperature. 2-Cyclopentenone (**4**) was selected as the substrate due to its smaller size and flat shape. Starting from the key [((*R,R*)-**IV**)Rh-Ph] intermediate (**12**), two competing pathways, one leading to (*R*)-**5** (R-pathway; **13**-**18**) and the other – to (*S*)-**5** (S-pathway; **19**-**23**), need to be followed for computational characterization of the enantioselectivity. The reaction coordinate in this part of the cycle can be approximated by the Rh-C_1 distance increasing from 2.003 Å in **12** to 4.334/4.010 Å in **18**/**23**, respectively, and the C_1-C_b decreasing from ∞ in **12** + **2** (the thermodynamic zero point) to 1.510/1.514 Å in **18**/**23**, respectively. The reaction coordinate interacts with selected dihedral/inter-bond angles (4-atomic coordinates); this is the origin of the fundamentally important phenomenon that conformation strongly perturbs stationary point energies hence the selectivity of the reaction. During the EB stage (before CR), the main perturbing dihedral angle to consider is D1 (C_1→Rh→C_a→C_b; Figure 2b); it can adopt up to 4 different values where local minima reside. D1 ~ 180° (syn-EB) corresponds to the Rh-Ph and C=C bond eclipsed in a way that places the Ph group near the ketone oxygen. Such orientation is unproductive for CR, and is expected to be the highest in energy. Therefore, such stationary points were not optimized. D1 ~ 0° (anti-EB) corresponds to the only "eclipsed" orientation in which CR can take place. Two other "perpendicular" orientations are possible, close-EB and far-EB,

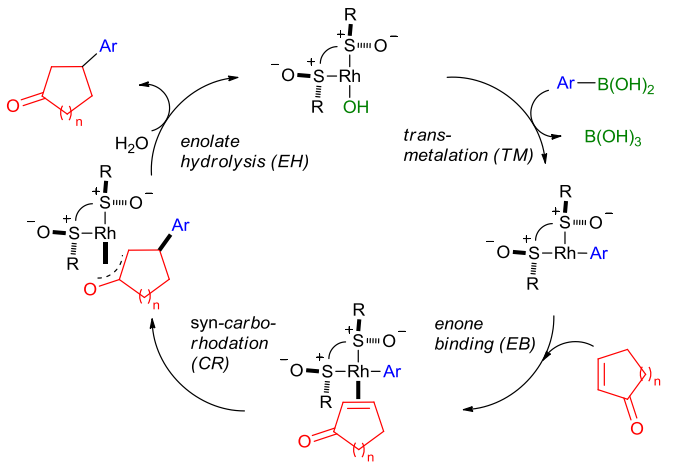

Scheme 2. The accepted catalytic cycle for the 1,4-aryltaion reaction with **IV** as the ligand (R = *t*-Bu).

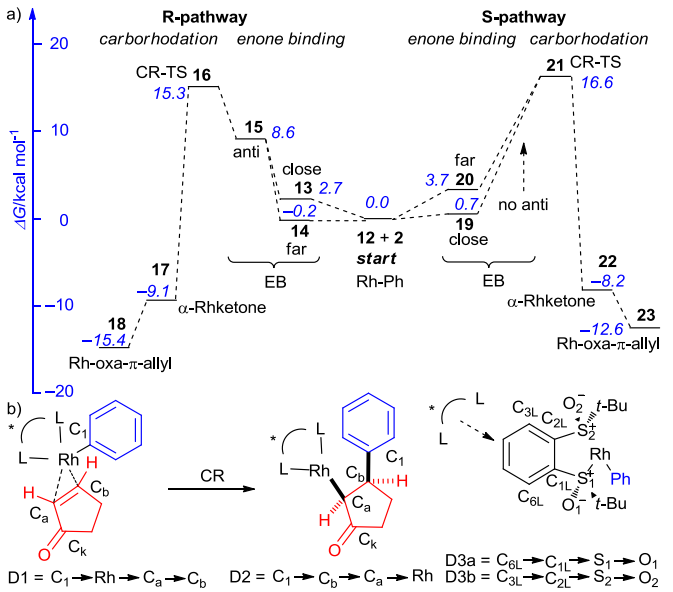

Figure 2. (a) The reaction profile for the EB+CR stages of the catalytic cycle (Scheme 2) calculated at IEFPCM (CH_2Cl_2, 313.15K)/PBE0/DGDZVP level of theory. (b) The main dihedral angles (D1-D3) that affect the reaction coordinate.

in which the Rh-phenyl eclipses the ketone ring, or is situated opposite, respectively. In the R-pathway, all 3 conformers were found (**13**-**15**), with the far-EB (**14**; D1 = –102°, ΔG = –0.2 kcal mol^{-1}) being the most stable and the anti-EB (**15**; D1 = –16°, ΔG = 8.6 kcal mol^{-1}) being the least stable, both for the whole profile. The close-EB (**13**; D1 = 92°, ΔG = 2.7 kcal mol^{-1}) is of intermediate stability as are the only 2 conformers found in the S-pathway, close-EB (**19**; D1 = –92°, ΔG = 0.7 kcal mol^{-1}) and

far-EB (**20**; D1 = 95°, ΔG = 3.7 kcal mol^{-1}), were found. All the EB intermediates were slightly distorted from the square-planar geometry typical for Rh(I) under the influence of the steric bulk of the neighbouring *t*-Bu group. However, alternative tetrahedral structures proved unstable. Note that in the Hayashi models (Figure 1b), the anti-EB conformer is explicitly shown. However, our calculations for various ligands, including **I**,[15] **II**,[15, 17] and now **IV** show that the EB step is highly variable, with the anti-EB conformers often being not the most stable, or not even existing at all.

Upon CR, the D2 dihedral angle ($C_1 \rightarrow C_b \rightarrow C_a \rightarrow Rh$; Figure 2b) becomes more chemically meaningful than D1. The R-pathway CR-TS (**16**; D1 = –23°, D2 = 27°, ΔG = 15.3 kcal mol^{-1}) is lower in energy than the S-pathway CR-TS (**21**; D1 = –18°, D2 = 21°, ΔG = 16.6 kcal mol^{-1}), correctly predicting the (*R*)-**5** as the major enantiomer in accord with the experiment. For the CR-TSs, we evaluated the effect of the *t*-Bu-sulfoxide rotation (dihedral angles D3a and b; Figure 2b). As expected, the *t*-Bu group showed a very strong tendency to move away from the plane (D3 ~ ±75°) of the *o*-benzylidene ring to avoid steric clash with the *o*-hydrogens. That signifies that ligand **IV** is not only bulky but also quite rigid. The CR-TSs collapse to a pair of α-Rhketones, in which the *syn*-periplanar orientation of the Ph and [(*R*,*R*)-**IV**)Rh] moieties is largely preserved (R-pathway, **17**, D2 = 5°, ΔG = –9.1 kcal mol^{-1}; S-pathway, **22**, D2 = 13°, ΔG = –8.2 kcal mol^{-1}). A sliding motion of the Rh atom towards the ketone oxygen completes the 1,4-addition by forming a pair of Rh-oxa-π-allyl complexes while simultaneously relieving Ph/Rh torsional strain as evidenced by the increasing D2 values, leading to additional free energy gain (R-pathway, **18**, D2 = 72°,ΔG = –9.1 kcal mol^{-1}; S-pathway, **23**, D2 = –29°,ΔG = –8.2 kcal mol^{-1}). The (*R*)-product is thus both kinetically and thermodynamically preferred.

The EB step being mildly exergonic to endergonic implies that all of the EB conformers will be in rapid equilibrium among each other, and with the uncomplexed Rh-Ph species and enone. In such a case, the chirality of the product is determined solely by the energies of the CR-TSs that follow. This finding is common among representatives of 3 main ligand classes, diphosphanes (**I**),[15] dienes (**II**)[15, 17] and disulfoxides (**IV**). Applying transition state theory to enantioselective catalysis[28] shows that the enantiomeric excess can be calculated from the difference of the Gibbs energies of two competing, diastereomeric CR-TSs ($\Delta\Delta G^{\ddagger} = \Delta G_{CR\text{-}TS}(R) - \Delta G_{CR\text{-}TS}(S)$):

$$ee\%\ (R) = \frac{\left(1 - e^{-\frac{\Delta\Delta G^{\ddagger}}{RT}}\right)}{\left(1 + e^{-\frac{\Delta\Delta G^{\ddagger}}{RT}}\right)} \times 100 \qquad (eq\ 1)$$

We calculated the required CR-TSs for all substrates in Scheme 1 with (*R*,*R*)-**IV**/Rh as the catalyst. The R- and S-pathways for substrates **1**, **6** and **8** are additionally split as a consequence of the conformational specifics of these substrates (Figure 3). The 6-member ring substrates 2-cyclohexenone (**1**) and 5,6-dihydro-2*H*-pyran-2-one (**6**) exist as a pair of inseparable chiral conformations, each of which can be distinguished by the Rh catalyst depending on the position of C_5 being on the same ("up") or the opposite ("down") side (middle). On the other hand, the linear (*E*)-3-penten-2-one (**8**) exists as a pair of diastereomeric *s-trans* and *s-cis* conformers (right). At IEFPCM(CH_2Cl_2, 313.15 K)/PBE0/DGDZVP level of theory, both conformers have equal energies. Therefore, for these substrates total of 4 CR-TSs each have to be calculated. 2-Cyclopentenone (**4**) or 4-chromenone (**10**), being flat, have no

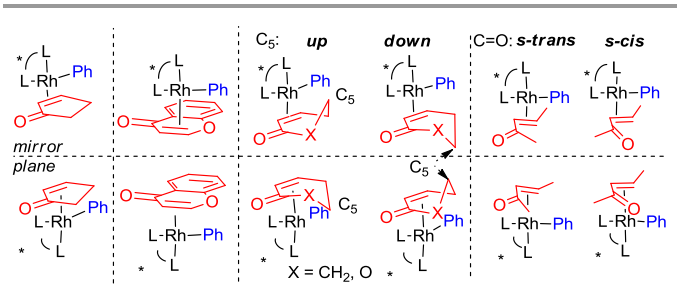

Figure 3. Effect of substrate conformations on the reaction pathways and the number of the associated CR-TSs.

inherent conformations (left) and only 2 CR-TSs have to be considered. The comparison of the theoretical and predicted enantioselectivities (Table 1) showed that for all cyclic (*Z*)-olefin substrates, the major enantiomer was (*R*) whereas for the linear (*E*)-olefin in 3-penten-2-one – (S). This suggests that that ligand (*R*,*R*)-**IV** exhibits the same sense of enantiodiscrimination as (R)-**I** and **II** and also indicates an excellent qualitative agreement between theory and experiment. Examination of the relative energies of the CR-TSs revealed that the chromenone lowest CR-TS (**36**) was 3.5 to 6.5 kcal mol^{-1} higher in energy than those for the smaller substrates (**16**, **24**, **28** and **34**, respectively). This indicates a lower rate of CR, which correlates well with the lower yield for this substrate under identical conditions (Scheme 1). Quantitatively, the IEFPCM/PBE0/DGDZVP model chemistry showed various degrees of accuracy. Interestingly, the theoretical enantioselectivities for the single-conformer cyclic substrates (**4** and **10**) were underestimated (by 0.8 and 1.2 kcal mol^{-1}, respectively), those for the up/down double conformer cyclic substrates (**1** and **6**) were overestimated (by 0.8 and 0.5 kcal mol^{-1}, respectively), and the one for the acyclic (*E*)-enone **8** was about right (0.2 kcal mol^{-1} underestimated). Inclusion of empirical correction for dispersion interactions, modelling of which is a traditional weakness of DFT, is often beneficial to improve quantitative agreement between experiment in theory.[29] Therefore, we reoptimized all structures involved in the enantioselectivity prediction with SMD/M06 method. SMD[30] is a recent parameterization variant of the PCM model including an improved set of van der Waals radii whereas M06[31] is a recent, general-purpose hybrid-meta-GGA functional parameterized to satisfy a number of constraints also containing 25% HF. Both methods include dispersion-interaction corrections. The reaction barriers ($\Delta G^{\ddagger}$) were systematically lowered with the SMD/M06 method (by 0.4-5.0 kcal mol^{-1}). However, the accuracy in $\Delta\Delta G^{\ddagger}$ hence predicted %ee improved considerably for the most problematic (for PCM/PBE0) substrates **4** and **10**. On the other hand, the accuracy for the linear (*E*)-enone **8** decreased, but remained within the 1 kcal mol^{-1} range (along with all other substrates) recently proposed as an acceptable accuracy at the current state-of-the-art in DFT modelling of enantioselectivity.[32] The origin of the discrepancies is unclear at present, but it underscores the significant challenges modelling of asymmetric catalysts pose to modern electronic structure theory. These findings are in line with our previous results for ligands **I**[15] and **II**[15, 17] for substrates **1** and **4** as well.

For all substrates, the CR-TSs adopt the distorted rectangular configuration characteristic for CR (migratory insertion) (Figure 4). It is noteworthy that for ligand **IV**, the original premise behind the Hayashi model, namely the avoidance of the steric clash between the large ligand

Journal Name

RSCPublishing

ARTICLE

Table 1. Comparison of the calculated and experimental enantioselectivities with traditional PCM/PBE0 and dispersion-interaction-corrected SMD/M06 methods (both with DGDZVP basis set).

s. m.[a]	PCM(CH_2Cl_2, 313.15K)/PBE0/DGDZVP				SMD(CH_2Cl_2, 313.15K)/M06/DGDZVP			
	ΔG (CR-TS), kcal mol^{-1}[b]		Enantioselectivity[c]		ΔG (CR-TS), kcal mol^{-1}[b]		Enantioselectivity[c]	
	R-pathway	S-pathway	theory	expt.	R-pathway	S-pathway	theory	expt.
1	15.9 (**24**); 17.4 (**25**)[d]	19.6 (**26**); 22.5 (**27**)[d]	–3.7 (99.5)	–2.9 (98)	11.5 (**24**); 13.5 (**25**)[d]	14.8 (**26**); 18.9 (**27**)[d]	–3.3 (99.0)	–2.9 (98)
4	15.3 (**16**)	16.6 (**21**)	–1.3 (78)	–2.2 (94)	14.4 (**16**)	16.2 (**21**)	–1.8 (89)	–2.2 (94)
6	13.8 (**28**); 18.9 (**29**)[d]	16.5 (**30**); 20.7 (**31**)[d]	–2.7 (97.6)	–2.2 (94)	9.9 (**28**); 14.3 (**29**)[d]	11.9 (**30**); 19.0 (**31**)[d]	–2.0 (92)	–2.2 (94)
8	15.5 (**32**); 18.9 (**33**)[e]	12.8 (**34**); 16.2 (**35**)[e]	2.7 (–97.5)	2.9 (–98)	11.0 (**32**); 13.9 (**33**)[e]	8.9 (**34**); 11.2 (**35**)[e]	2.1 (–93)	2.9 (–98)
10	19.3 (**36**)	21.4 (**37**)	–2.1 (93)	–3.3 (99)	14.3 (**36**)	17.2 (**37**)	–2.9 (98)	–3.3 (99)

[a]S. m. = starting material (Scheme 1). [b]Relative to ΔG(**12**) + ΔG(s.m.). [c]Given in kcal mol^{-1} (%ee) and positive for the (*R*)-enantiomer. The two values were interconverted according eq.1. [d]"Up"; "down", respectively. [d]"*s-cis*"; "*s-trans*", respectively.

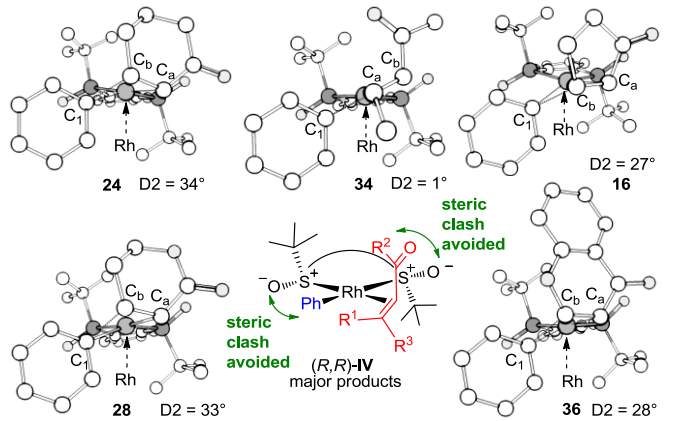

Figure 4. The optimized structures of the CR-TSs for all substrates (Table 1) leading to the major products. A Hayashi-type model consistent with both theoretical and experimental enantiodiscrimination is readily conceived from these structures.

substituent (*t*-Bu in this case) and the ketone substituent is still substituent on the opposite face of the plane. This second instance of steric clash avoidance is not a feature of the original Hayashi model. Based, on the DFT results, we can propose a pictorial model (Figure 4, middle, down) that embodies the idea of Liao et al., who concluded, based on the X-ray structure of the [((*R*,*R*)-**IV**)RhCl]$_2$ complex, "the two *tert*-butyl groups provide an excellent stereoenvironment that may generate the high enantioselectivity in the 1,4-addition".[22]

In the above model, the ketone finds in a close proximity to the sulfoxide oxygen atom. Recall that the enantioselectivity of biaryl-derived sulfoxides was presumed to have been governed by the repulsion of the sulfoxide and ketone oxygens (Figure 1b). Multiple weak interactions were found in the Atoms-In-Molecules (AIM)[33] wavefunction analyzes (Figure 5) of the two competing CR-TSs for 2-cyclopentenone (**16** and **21**), indicative of van der Waals interactions arising from steric hindrance. There is a weak interaction (ρ_b = 0.0050) in the major R-CR-TS (**16**), between the ketone oxygen and the sulfoxide oxygen that corresponds to the predicted dipole-dipole repulsion. However, it appears that the high steric valid, despite both *t*-Bu group and O atom pointing slightly backwards from the plane where the two S atoms lie. The high steric pressure exercised by the *t*-Bu groups is evident in the uneven, and at times quite large, degree of geometric distortion imposed on the key CR-TS structure encompassing C_1, C_a, C_b, and Rh, and D2 dihedral angle these atoms form. The 6-member, non-planar substrates (**1** and **6**) are the most distorted (D2 = 34 and 33°, respectively) due to the steric clash between the C_5-CH_2 group sticking up, towards the *t*-Bu group on the opposite S atom (Figure 4, left). On the other hand, the linear (*E*)-enone **8** fits very snugly between the two C_2-symmetrical *t*-Bu groups, resulting in a very small D2 angle (1°) (Figure 4 middle, up). The situation with the flat cyclic substrates (**4**, **10**) is intermediate (D2 = 27 and 28°, respectively; Figure 4, right). Note that in all of the above structures, the Rh-phenyl group is pushed out of the Rh coordination plane by the bulky S-*t*-Bu pressure exercised by the *t*-Bu groups dominates. In that sense, ligand **IV** is similar to **I**, another high steric pressure[15] ligand.

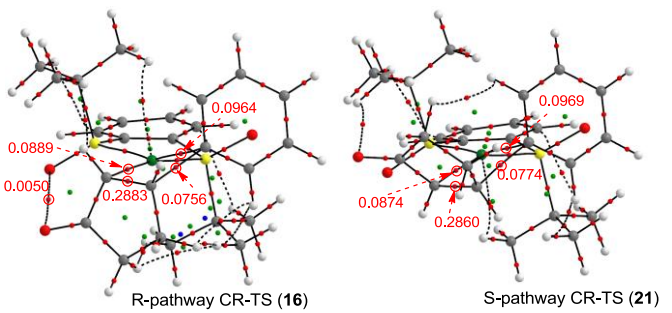

Figure 5. AIM plots for the two competing CR-TSs for 2-cyclopentenone. The criticial points (CPs) are shown as follows: bond (B), red; ring (R), green; and cage (C), blue. Selected BCP electron densities (ρ_b) are also shown.

Conclusions

The enantioselective step in the 1,4-addition of phenylboronic acid to a variety Michael acceptors catalyzed Rh ligated with a disulfoxide ligand whose only source of chirality is the sulfur atoms was modelled by DFT (PCM/PBE0/DGDZVP level of theory). For all substrates, the predicted absolute configuration agreed with the experiment. However, the calculated %ee over-

or underestimated the experimental values. The high steric pressure exercised by the two *t*-Bu groups dominates over the weaker dipole-dipole repulsion between the ketone and sulfoxide O atom, and is the primary determinant of the enantioselectivity.

Acknowledgements

This work was supported by Hefei University of Technology, The Natural Sciences Foundation of Anhui Province (grant 11040606M35) and Wuhan University of Technology (China) and Institute of Materials Research and Engineering, A*STAR, (Singapore). The authors thank A*STAR Computational Resources Centre (Singapore) for the generous gift of computational time on the Axle, Fuji, Cirrus and Aurora HPC clusters.

Notes and references

[a] *School of Chemistry and Chemical Engineering, Hefei University of Technology, 193 Tunxi Road, Hefei 230009, China. Fax: ++86-551-6290-1450; Tel: ++86-551-6290-1450; E-mail: liyg@hfut.edu.cn, ekantchev@hfut.edu.cn, ekantchev@gmail.com*
[b] *School of Chemistry, Chemical Engineering and Biological Science, Wuhan University of Technology, 205 Luoshi Road, Wuhan, 430070, China*
[c] *Former address: Institute of Materials Research and Engineering, 3 Research Link, Singapore 117602*

† Electronic Supplementary Information (ESI) available: Cartesian coordinates, energies and first 3 frequencies for all stationary points and IRC plots for selected transition states. See DOI: 10.1039/b000000x/

1. E. N. Jacobsen, A. Pfaltz and H. Yamamoto, eds., *Comprehensive asymmetric catalysis*, Springer, Berlin, 1999.
2. H. J. Edwards, J. D. Hargrave, S. D. Penrose and C. G. Frost, *Chem. Soc. Rev.*, 2010, **39**, 2039-2105.
3. G. Berthon and T. Hayashi, in *Catalytic Asymmetric Conjugate Reactions*, ed. C. A, Wiley-VCH, 2010, pp. 1-70.
4. M. Sakai, H. Hayashi and N. Miyaura, *Organometallics*, 1997, **16**, 4229-4231.
5. Y. Takaya, M. Ogasawara, T. Hayashi, M. Sakai and N. Miyaura, *J. Am. Chem. Soc.*, 1998, **120**, 5579-5580.
6. (a) T. Hayashi, K. Ueyama, N. Tokunaga and K. Yoshida, *J. Am. Chem. Soc.*, 2003, **125**, 11508-11509; Simultaneously an dindependently, a C_1-symmetrical chiral diene was developed for the Ir-catalyzed allylic substitution reaction: (b) C. Fischer, C. Defieber, T. Suzuki and E. M. Carreira, *J. Am. Chem. Soc.*, 2004, **126**, 1628-1629.
7. (a) A. Kina, H. Iwamura and T. Hayashi, *J. Am. Chem. Soc.*, 2006, **128**, 3904-3905; (b) A. Kina, Y. Yasunara, T. Nishimura, H. Iwamura and T. Hayashi, *Chem. Asian J.*, 2006, **1**, 707-711.
8. (a) P. Tian, H.-Q. Dong and G.-Q. Lin, *ACS Catal.*, 2012, **2**, 95-119; (b) T. Hayashi and K. Yamasaki, *Chem. Rev.*, 2003, **103**, 2829-2844; (c) K. Fagnou and M. Lautens, *Chem. Rev.*, 2003, **103**, 169-196.
9. R. Mariz, X. Luan, M. Gatti, A. Linden and R. Dorta, *J. Am. Chem. Soc.*, 2008, **130**, 2172-2173.
10. J. J. Bürgi, R. Mariz, M. Gatti, E. Drinkel, X. Luan, S. Blumentritt, A. Linden and R. Dorta, *Angew. Chem., Int. Ed.*, 2009, **48**, 2768-2771.
11. F. Ozawa, A. Kubo, Y. Matsumoto, T. Hayashi, K. Nishioka, K. Yanagi and K. Moriguchi, *Organometallics*, 1993, **12**, 4188-4196.
12. G. Berthon-Gelloz and T. Hayashi, *J. Org. Chem.*, 2006, **71**, 8957-8960.
13. (a) T. Nishimura, A. Noishiki, C. C. Tsui and T. Hayashi, *J. Am. Chem. Soc.*, 2012, **134**, 5056-5059; (b) K. Sasaki, T. Nishimura, R. Shintani, E. A. B. Kantchev and T. Hayashi, *Chem. Sci.*, 2012, **3**, 1278-1283; (c) D. W. Low, G. Pattison, M. D. Wieczysty, G. H. Churchill and H. W. Lam, *Org. Lett.*, 2012, **14**, 2548-2551; (d) Y. Luo, H. B. Hepburn, N. Chotsaeng and H. W. Lam, *Angew. Chem., Int. Ed.*, 2012, **51**, 8309-8313; (e) Y. Luo, A. J. Carnell and H. W. Lam, *Angew. Chem., Int. Ed.*, 2012, **51**, 6762-6766; (f) J. Csizmadiová, M. Mečiarová, E. Rakovský, B. Horváth and R. Šebesta, *Eur. J. Org. Chem.*, 2011, 6110-6116; (g) A. Saxena and H. W. Lam, *Chem. Sci.*, 2011, **2**, 2326-2331; (h) R. Shintani and T. Hayashi, *Org. Lett.*, 2011, **13**, 350-352; (i) R. Shintani, M. Takeda, Y.-T. Soh, T. Ito and T. Hayashi, *Org. Lett.*, 2011, **13**, 2977-2979; (j) R. Shintani, S. Isobe, M. Takeda and T. Hayashi, *Angew. Chem., Int. Ed.*, 2010, **49**, 3795-3798; (k) G. Pattison, G. Piraux and H. W. Lam, *J. Am. Chem. Soc.*, 2010, **132**, 14373-14375; (l) T. Nishimura, H. Makino, M. Nagaosa and T. Hayashi, *J. Am. Chem. Soc.*, 2010, **132**, 12865-12867; (m) C. Shao, H.-J. Yu, N.-Y. Wu, C.-G. Feng and G.-Q. Lin, *Org. Lett.*, 2010, **12**, 3820-3823; (n) T. Gendrineau, O. Chuzel, H. Eijsberg, J.-P. Genet and S. Darses, *Angew. Chem., Int. Ed.*, 2008, **47**, 7669-7672; (o) K. Okamoto, T. Hayashi and V. H. Rawal, *Org. Lett.*, 2008, **10**, 4378-4389; (p) F. Läng, F. Breher, D. Stein and H. Grützmacher, *Organometallics*, 2005, **24**, 2997-3007; (q) N. Tokunaga, Y. Otomaru, K. Okamoto, K. Ueyama, R. Shintani and T. Hayashi, *J. Am. Chem. Soc.*, 2004, **126**, 13584-13585.
14. Q. Chen, C. Chen, F. Guo and W. Xia, *Chem. Commun.*, 2013, **49**, 6433-6435.
15. H.-L. Qin, X.-Q. Chen, Y.-Z. Huang and E. A. B. Kantchev, *Chem. Eur. J.*, 2014, **20**, 12982-12987.
16. (a) T. Korenaga, R. Maenishi, K. Hayashi and T. Sakai, *Adv. Synth. Catal.*, 2010, **352**, 3247-3254; (b) P. Mauleon, I. Alonso, M. Rodriguez Rivero and J. C. Carretero, *J. Org. Chem.*, 2007, **72**, 9924-9935; (c) T. Itoh, T. Mase, T. Nishikata, T. Iyama, H. Tachikawa, Y. Kobayashi, Y. Yamamoto and N. Miyaura, *Tetrahedron*, 2006, **62**, 9610-9621.
17. E. A. B. Kantchev, *Chem. Sci.*, 2013, **4**, 1864-1875.
18. (a) S. Gosiewska, J. A. Raskatov, R. Shintani, T. Hayashi and J. M. Brown, *Chem. Eur. J.*, 2012, 80-84; (b) E. A. B. Kantchev, *Chem. Commun.*, 2011, **47**, 10969-10971.
19. (a) A. Poater, F. Ragone, R. Mariz, R. Dorta and L. Cavallo, *Chem. Eur. J.*, 2010, **16**, 14348-14353; (b) R. Mariz, A. Poater, M. Gatti, E. Drinkel, J. J. Bürgi, X.-J. Luan, S. Blumentritt, A. Linden, L. Cavallo and R. Dorta, *Chem. Eur. J.*, 2010, **16**, 14335-14347.
20. (a) E. Ichikawa, M. Suzuki, K. Yabu, M. Albert, M. Kanai and M. Shibasaki, *JACS*, 2004, **126**, 11808-11809; (b) R. Tokinoh, M. Sodeoka, K. Aoe and M. Shibasaki, *Tetrahedron Lett.*, 1995, **44**, 8035-8038; (c) N. Khiar, I. Fernández and A. F, *Tetrahedron Lett.*, 1993, **34**, 123-126; (d) B. R. James and R. S. McMillan, *Can. J. Chem.*, 1977, **55**, 3927-2932.
21. (a) N. Khiar, A. Salvador, V. Valdivia, A. Chelouan, Alcudia, E. Álvarez and I. Fernández, *J. Org. Chem.*, 2013, **78**, 6510-6521; (b) H. F, C. G, X. Zhang and J. Liao, *Eur. J. Org. Chem.*, 2011, 2928-2931; (c) P. K. Dornan, P. L. Leung and V. M. Dong, *Tetrahedron*, 2011, **67**, 4378-4384. (d) Q.-A. Chen, X. Dong, M.-W. Chen, D.-S. Wang, Y.-G. Zhou and Y.-X. Li, *Org. Lett.*, 2010, **12**, 1928-1931;

22. J. Chen, J. Chen, F. Lang, X. Zhang, L. Cun, J. Zhu, J. Deng and J. Liao, *JACS*, 2010, **132**, 4552-4553.
23. T. Hayashi, M. Takahashi, Y. Takaya and M. Ogasawara, *J. Am. Chem. Soc*., 2002, **124**, 5052-5058.
24. M. J. Frisch, G. W. Trucks, H. B. Schlegel, G. E. Scuseria, M. A. Robb, J. R. Cheeseman, G. Scalmani, V. Barone, B. Mennucci, G. A. Petersson, H. Nakatsuji, M. Caricato, X. Li, H. P. Hratchian, A. F. Izmaylov, J. Bloino, G. Zheng, J. L. Sonnenberg, M. Hada, M. Ehara, K. Toyota, R. Fukuda, J. Hasegawa, M. Ishida, T. Nakajima, Y. Honda, O. Kitao, H. Nakai, T. Vreven, J. A. Montgomery, Jr., J. E. Peralta, F. Ogliaro, M. Bearpark, J. J. Heyd, E. Brothers, K. N. Kudin, V. N. Staroverov, R. Kobayashi, J. Normand, K. Raghavachari, A. Rendell, J. C. Burant, S. S. Iyengar, J. Tomasi, M. Cossi, N. Rega, N. J. Millam, M. Klene, J. E. Knox, J. B. Cross, V. Bakken, C. Adamo, J. Jaramillo, R. Gomperts, R. E. Stratmann, O. Yazyev, A. J. Austin, R. Cammi, C. Pomelli, J. W. Ochterski, R. L. Martin, K. Morokuma, V. G. Zakrzewski, G. A. Voth, P. Salvador, J. J. Dannenberg, S. Dapprich, A. D. Daniels, Ö. Farkas, J. B. Foresman, J. V. Ortiz, J. Cioslowski, and D. J. Fox, *Gaussian 09, Revision A.02*.
25. J. P. Perdew, K. Burke and M. Ernzerhof, *Phys. Rev. Lett.*, 1996, **77**, 3685-3868; errata: ibid, 1997, **78**, 1396.
26. N. Godbout, D. R. Salahub, J. Andzelm and E. Wimmer, *Can. J. Chem.*, 1992, **70**, 560-571.
27. J. Tomasi, B. Mennucci and R. Cammi, *Chem. Rev.*, 2005, **105**, 2999-3093 and refs. cited therein.
28. D. Balcells and F. Maseras, *New J. Chem.*, 2007, **31**, 333-343.
29. (a) S. Ehrlich, J. Moellmann and S. Grimme, *Acc. Chem. Res.*, 2013, **46**, 916-926; (b) S. Grimme, *Wiley Interdisc. Rev. Comp. Mol. Sci.*, 2011, **1**, 211-228; (c) T. Schwabe and S. Grimme, *Acc. Chem. Res.*, 2008, **41**, 569-579.
30. A. V. Marenich, C. J. Cramer and D. Truhlar, *J. Phys. Chem. B*, 2009, **113**, 6378-6396.
31. Y. Zhao and D. G. Truhlar, *Theor. Chem. Account.*, 2008, **120**, 215-241.
32. A. Armstrong, R. A. Boto, P. Dingwall, J. Contreras-García, M. J. Harvey, N. J. Mason and H. S. Rzepa, *Chem. Sci.*, 2014, **5**, 2057-2071.
33. For a general introduction, see: (a) R. F. W. Bader, *Atoms in Molecules: A Quantum Theory*, Clarendon Press, Oxford, UK, 1990. The AIM calculations were performed with AIMAll software: T. A. Keith, TK Gristmill Software, Overland Park KS, USA, 2014.

Graphical abstract